Non-flutter design principle for twin boxes

Michael Styrk Andersen[1], Jesper Røssel Læsø[2], Michael Lenius[2], Jens Johansson[3]
[1]Ph.D. Student, Faculty of Engineering, University of Southern Denmark, Campusvej 55 Odense, Denmark
[2]Student M.Sc. Eng., Faculty of Engineering, University of Southern Denmark, Campusvej 55 Odense, Denmark
[3]Assistant professor, Ph.D., Faculty of Engineering, University of Southern Denmark, Campusvej 55 Odense, Denmark
Email: mian@iti.sdu.dk, jensj@iti.sdu.dk

ABSTRACT: Cable supported bridges may become aerodynamically unstable at low wind velocities if they are not designed properly. Increasing spans generally reduces the critical flutter wind velocity due to a reduction in the torsional-to-vertical frequency ratio of the bridge deck. Within flat plate aerodynamics it is though well known that classical flutter cannot occur if the torsional natural frequency is lower than the vertical. In this paper, free vibration tests of a section model composed of two boxes each with a depth-to-width ratio $D:B = 1:12$ is analyzed at torsional-to-vertical frequency ratios above and below unity. Classical flutter did not occur for the twin boxes having torsional-to-vertical frequency ratio below 1. These results support the non-flutter design principle. At a frequency ratio of approximately 1.20 the twin boxes and a reference flat plate model having $D:B = 1:24$ is compared. The twin boxes obtained a higher critical velocity than the reference flat plate model. Aerodynamic Derivatives identified from the tests are compared for the twin boxes and the flat plate. Negative aerodynamic torsional stiffness is less pronounced for the twin boxes compared with the flat plate while the aerodynamic torsional damping is positive and larger. Aerostatic moment coefficients of the twin boxes were identified from the free vibration tests at different angles of attack close to the critical torsional divergence velocity. The slope of the moment coefficients identified for the twin boxes at different angles of attack is considerable below that of a flat plate. Therefore the critical velocities for torsional divergence may be expected to be higher for twin boxes compared with flat plates. This may pave the way for aerodynamically and aerostatically stable twin bridge designs with low torsional frequencies in the future.

KEY WORDS: Bridge Aerodynamics; Twin Boxes, Flat plates, Aerodynamic Derivatives, Torsional Divergence

NOMENCLATURE

α, h	Torsional and vertical degrees of freedom.
ω_α, ω_h	Torsional and vertical angular frequency
f_α, f_h	Torsional and vertical frequency
ζ_α, ζ_h	Torsional and vertical damping ratios
k_α, k_h	Torsional and vertical stiffness
m_e, I_e	Modal mass – and mass moment of inertia per unit length
f, ω	Frequency in Hz and angular frequency in rad/s.
γ_ω	Torsional-to-vertical frequency ratio
ρ	Density of air
D, B, L, Z	Depth, width, length and gap of section model
e_k	Spring eccentricity
t	Time
$C_m(\alpha)$	Coefficient for the aerodynamic moment
F_M, F_D, F_L	Aerodynamic moment, drag and lift force
$C_m{}'$	Slope of the aerodynamic moment coefficient curve at $\alpha = 0$.
H_i^*, A_i^*	Aerodynamic derivatives (AD's)
U, I_u	Wind velocity and along wind turbulence intensity
U_{TD}	Critical wind velocity for torsional divergence
U_r	Reduced non-dimensional wind velocity
U_{CL}	Reduced critical wind velocity for classic flutter
$U_{TD,R}$	Reduced critical wind velocity for torsional divergence
U_1, U_2	Highest observed reduced non-critical wind velocity and smallest observed reduced critical wind velocity
U_{cr}	Reduced critical wind velocity for either flutter or torsional divergence

1 INTRODUCTION

The design procedures implemented in bridge engineering after the dramatic collapse of the first Tacoma Narrows Bridge in 1940, includes the investigation of various aeroelastic phenomena, e.g. flutter of the bridge deck in its final stage. Bridge deck flutter is a dynamic instability caused by the motion induced wind load of the bridge deck when it is subjected to cross winds. The displacements are characterized by harmonic angular displacements, which increase for each oscillation cycle and eventually lead to structural failure.

The coupling of torsional and vertical modes of long span bridges with a single bridge deck has been known to cause dynamic instability in terms of classical flutter since the Tacoma Narrows investigations, see e.g. Bleich, McCullough, Rosecrans, and Vincent (1950). The torsional stiffness of the bridge deck girder does usually ensure that the torsional frequency is considerably higher than the vertical frequency and thus postpones the onset of flutter to higher wind velocities. The effect of the torsional deck stiffness decreases when the span increases. For very long bridges this means that the torsional and vertical modes become very closely spaced. As the aerodynamic stiffness tends to decrease the torsional frequency in wind, the aerodynamic coupling between vertical and torsional modes is unavoidable. However, if the torsional still air frequency is below the vertical still air frequency, the modes will be decoupled with increasing frequency separation at higher wind velocities.

At the same time aerostatic instability in terms of torsional divergence must be prevented by sufficient torsional stiffness and an aerodynamic design that seeks to decrease the slope of the static aerodynamic torsional moment coefficient $C_m{}'$.

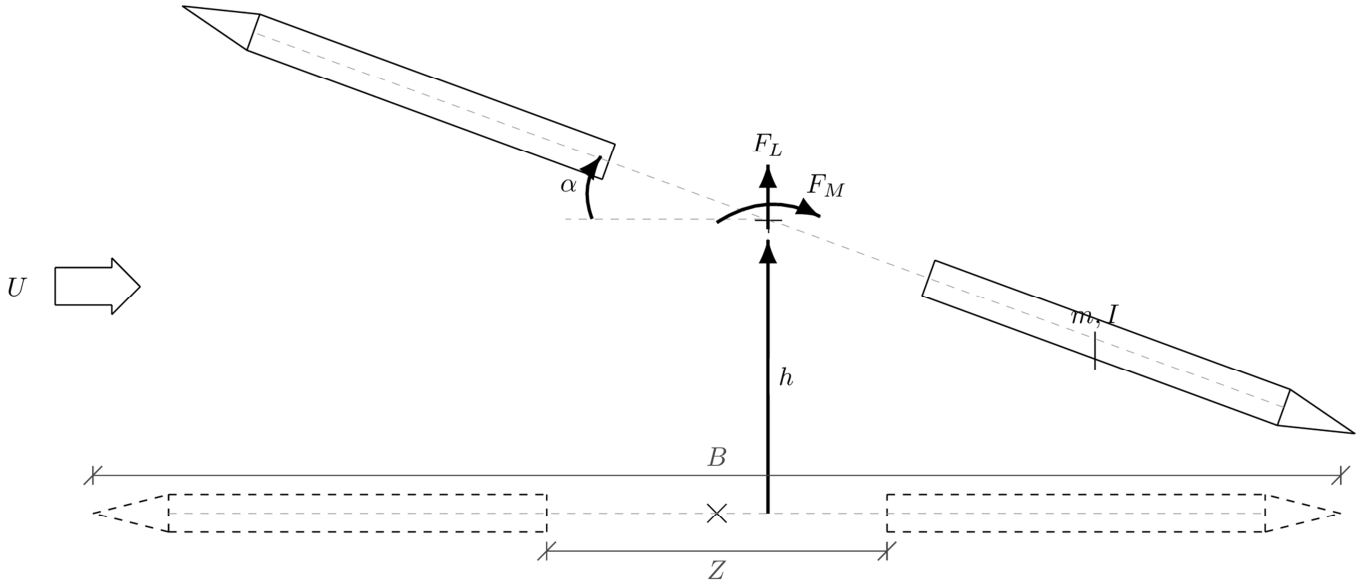

Figure 1: Section model cross sectional properties

Classical flutter was first observed in the aerospace industry, where the critical flutter wind velocity for a theoretical thin airfoil was derived by Theodorsen (1934). Bleich et al. (1950) adopted this approach to Bridge decks. Bridge deck flutter was later distinguished from airfoil flutter with the introduction of 6 bridge deck aerodynamic derivatives (AD's), H_i^*, A_i^* where $i = 1-3$ by Scanlan and Tomko (1971). The AD's determine the change in stiffness and damping due to the motion induced wind load which may lead to flutter. In the last decades, much effort has been put into the identification of 8 $(i = 1-4)$ and eventually 18 AD's. Several authors, e.g. and Chowdhury and Sarkar (2003), introduced techniques to identify the 18 AD's for bridge decks, but also stressed the difficulties in doing so. System identification algorithms using least squares techniques have also been developed to identify the AD's, see e.g. Ding, Zhou, Zhu, and Xiang (2010) and Gu, Zhang, and Xiang (2000).

The effect of gap width for twin boxes has been studied by Qin, Kwok, Fok, Hitchcock, and Xu (2007). They found that the AD's for twin boxes were sensitive to the gap width, especially torsional aerodynamic damping and stiffness, A_2^* and A_3^* respectively. They reported that a gap width of 16% of the total section width increases the positive torsional aerodynamic damping compared to zero gap width. A gap width of 35% offered no further improvement. The effect of torsional-to-vertical frequency ratio for twin boxes was studied by (Qin, Kwok, Fok, & Hitchcock, 2006). Deviations were found for A_2^* and A_3^*. However, no experiments with torsional-to-vertical frequency ratios below 1 were reported.

A mathematical description of the AD's effect on the motion-induced wind load of a bridge deck is given in the literature; see e.g. Dyrbye and Hansen (1997). If the sign of A_2^* and A_3^* are identical with those of a flat plate, classical flutter is prevented if the frequency ratio is below a certain limit determined by the structural damping. For zero structural damping, this limit is unity when using the theoretical flat plate AD's. In reality, i.e. with structural damping present, the limit will typically be approximately 1.1. Torsional flutter is prevented if the A_2^* values are all negative.

Richardson (1981) published the idea of twin suspension bridges with frequency ratios below unity. He indicated that twin-deck configurations are the most favorable for long span bridges and proposed a twin bridge with four main cables and a frequency ratio below unity as an economical and aerodynamically stable alternative to the single box girder suspension bridges. A twin box suspension bridge may however also be obtainable with only two main cables. Bartoli et al. (2008) tested a twin box configuration with torsional-to-vertical frequency ratios below 1. Classical flutter was not observed in the reported section model tests and torsional divergence did not occur until very high wind velocities were reached. They made a finite element model of a twin bridge configuration having two main cables and the deck external to the cable planes. They reported that the torsional-to-vertical frequency ratio was below 1 for the first symmetric and antisymmetric pairs of torsional twisting and vertical bending mode shapes. A similar design of a twin bridge with decks external to the cables was illustrated in Walshe and Wyatt (1992), but they did not report results from finite element models or wind tunnel tests.

Classical flutter can only occur between torsional and vertical modes of similar shape. Some of the present authors presented a detailed study of the mode shape similarity and the respective torsional-to-vertical frequency ratios between all possible combinations of the first 5 torsional and vertical modes of a twin bridge spanning 3700m in Andersen, Sahin, Laustsen, Lenius, and Røssel (2014). It was concluded that classical flutter is not likely to occur for modes of higher order if the torsional-to-vertical frequency ratio between the first symmetric modes is below 1.

Larsen and Larose (2015) wrote that a flutter-free design can be obtained for long span bridges if the torsional natural frequency is lower than the vertical bending natural frequency, but suggested that further insight is needed in relation to e.g. torsional divergence before this design principle can mature.

For the theoretical flat plate AD's, there is no solution to the critical flutter wind velocity for frequency ratios below unity. Some of the present authors investigated a single box $D{:}B = 1{:}10$ with γ_ω deliberately below unity in Johansson, Andersen, and Øvre (2013). In wind tunnel tests, the section model performed stable at frequency ratios $\gamma_\omega < 1$, while classical flutter was observed for frequency ratios above unity as expected.

The present study considers a geometrically very simple twin-deck configuration of two sharp edged rectangular boxes without railings, but with fairings at the outermost windward and leeward edges. The section model is illustrated in Figure 1.

It is well known that flat plate sections with frequency ratios above, but close to one are prone to flutter at low wind velocities. In this paper we present the twin-deck section model behavior at a range of torsional-to-vertical frequency ratios above and below unity. A reference to flat plate aerodynamics is done by testing the twin boxes right beside each other, i.e. with no central gap. The cross section used in the test Series is illustrated in Figure 2 and Figure 3.

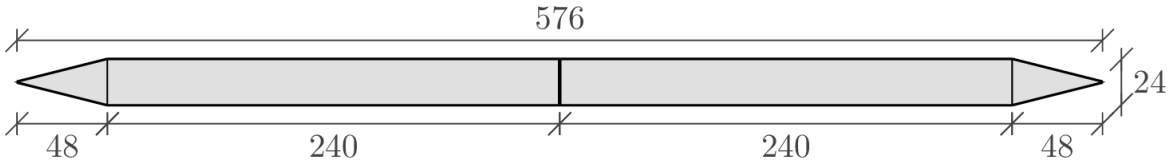

Figure 2: Cross section for test Series 1a and 1b. Dimensions are in 10^{-3} m.

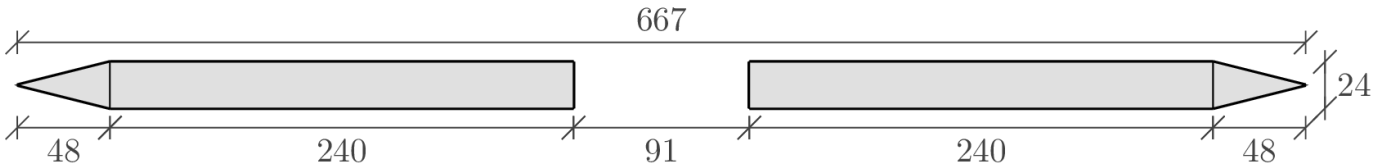

Figure 3: Cross section for test Series 2a, 2b and 2c. Dimensions are in 10^{-3} m.

The methods used to calculate the critical torsional divergence and classical flutter wind velocities are briefly introduced in Section 2.1 and 2.2 respectively. The wind tunnel and the test rig are present in Section 3 together with the methods used in the data processing. Time histories at the critical wind velocities, spectra of the model response at different wind velocities, aerostatic moment coefficients and the AD's for the flat plate and the twin boxes are presented in Section 4.

2 THEORY

Wind loading of bridges is distinguished in the static wind load and the motion induced wind load. The former may cause torsional divergence while the latter may cause flutter. Torsional flutter is known to occur for bluff rectangular section while classical flutter is feared because it also occurs for more streamlined sections. Multi-mode flutter may occur for deep sections prone to lateral wind forces.

2.1 Aerostatic stability

The static force equilibrium of the aerodynamic moment and the section model is given by Equation (1), where k_α is the torsional stiffness of the section model, ρ is the density of air, U is the mean wind velocity, B is the section model width and $C_m(\alpha)$ is the aerodynamic torsional moment coefficient at the angle of attack α.

$$k_\alpha \alpha = \frac{1}{2}\rho U^2 B^2 C_m(\alpha) \tag{1}$$

In the wind tunnel tests conducted, the torsional stiffness and the torsional displacement was measured. The torsional displacement was assumed to be equal to the angle of attack. One twin box section with low torsional stiffness rotated linearly with the mean wind velocity. The aerodynamic moment coefficient was identified from these tests according to Equation (2).

$$C_m(\alpha) = \frac{2k_\alpha \alpha}{\rho\, B^2 U^2} \tag{2}$$

The critical torsional divergence velocity occurs due to second order effects of the rotation of the section model. The torsional stiffness and the slope of the static aerodynamic torsional moment coefficient, $C_m{}'$ is determining for the critical divergence velocity U_{TD}. A theoretical flat plate has $\mathrm{C_m}' = \frac{\pi}{2}$ according to Dyrbye & Hansen (1997).

$$U_{TD} = \left(\frac{2k_\alpha}{\rho\, B^2 C_m{}'}\right)^{\frac{1}{2}} \tag{3}$$

As the span of cable supported bridges increases, the torsional stiffness of the girder decreases as these parameters are inverse proportional. Therefore, very long span bridges must minimize $C_m{}'$ and obtain high torsional stiffness by having sufficient spacing between the main cables as the torsional stiffness contribution from the girder decreases.

2.2 Aerodynamic stability

Cable supported bridges are flexible structures that responds to the wind in a dynamic manner. The motion induced forces determines the wind load on the bridge deck due to the displacements and velocity of the bridge deck itself. These loads are determined by the AD's.

The modal still air mass, damping and stiffness properties facilitate an equation of equilibrium with the motion-induced wind loads that are functions of the mean wind velocity, the frequency of oscillation and the section width. The mathematical description of this is given in e.g. Dyrbye & Hansen (1997) together with a solution procedure. An alternative solution procedure is to formulate the motion induced forces as aerodynamic damping and aerodynamic stiffness respectively. The wind velocity is conveniently described by the non-dimensional reduced wind velocity $U_r = U/(B\omega)$ where ω is the angular frequency of the bridge deck at the wind velocity U. The aerodynamic damping and stiffness described by the AD's and the reduced wind velocity on the right-hand side of the equation of motion is subtracted from the structural damping and structural stiffness on the left-hand side. The complex eigenvalues of the characteristic equation may now be evaluated at increasing reduced wind velocities until the real part becomes zero. This reduced velocity is the reduced critical flutter wind velocity where the absolute value of the damping is zero. At higher wind velocities the damping is expected to become negative and diverging oscillations will occur until structural collapse. A MATLAB routine of the latter approach has been implemented to calculate U_{CL}.

3 EXPERIMENTAL SETUP AND DATAPROCESSING

The experiments have been performed in the wind tunnel at Svend Ole Hansen ApS in Copenhagen. The wind tunnel is a boundary layer tunnel of the open return flow type having a $1.7m\ x\ 1.5m$ test section and a maximum tunnel velocity approximately equal to 12 m/s. The longitudinal turbulence intensity I_u measured was between 1% and 2% in the tests conducted.

Figure 4 shows the experimental model-rig system. Two identical section models with depth-to-width ratios $D{:}B = 1{:}12$ and adjustable gap-to-width ratios spans across the wind tunnel. Outside the wind tunnel, a horizontal bar connected to the model via a central rod, is suspended from springs at configurable positions. The spring eccentricity can be adjusted to the desired torsional rigidity. Dummy masses at the horizontal bar allows configuration of the mass moment of inertia through their eccentricity to the centre of gravity. Hence, the spring and dummy mass configuration determines the torsional natural frequency, and the torsional-to-vertical frequency ratio.

The transient vibration tests were executed with a combined vertical and torsional initial displacement at approximately $h = 5 * 10^{-3}m$ and $\alpha = 0.5 - 1.2°$ through all the tests. In order to avoid rolling motion, the natural frequency of the rolling mode was separated from the vertical and torsional natural frequencies. Furthermore, the initial displacements of the section model were carefully adjusted prior to the execution in order to avoid initiating rolling motion. An electromagnetic release mechanism was used to release the model simultaneously at the same initial conditions on both side of the tunnel through all

tests. Only the torsional and vertical degrees of freedom were of interest. Therefore drag wires prevented the section model from lateral motion.

Four of the performed Test Series are presented here. Table 1 summarizes the physical properties along with the experimental results. Test Series 1a is the reference flat plate with a frequency ratio of 1.2. In Test Series 2a a gap width, Z, of 13.64% of the total section model width, B, was introduced. The model had a torsional-to-vertical frequency ratio almost identical to test Series 1a. Special end brackets were used which allowed the adjustment of the gap width. Test Series 2b was similar to 2a except that the spring eccentricity was reduced in order to obtain a frequency ratio of 0.91. In Test Series 2c the spring eccentricity was equal to 2a. The frequency ratio of 0.99 was obtained by increasing the mass and mass moment of inertia using dummy masses.

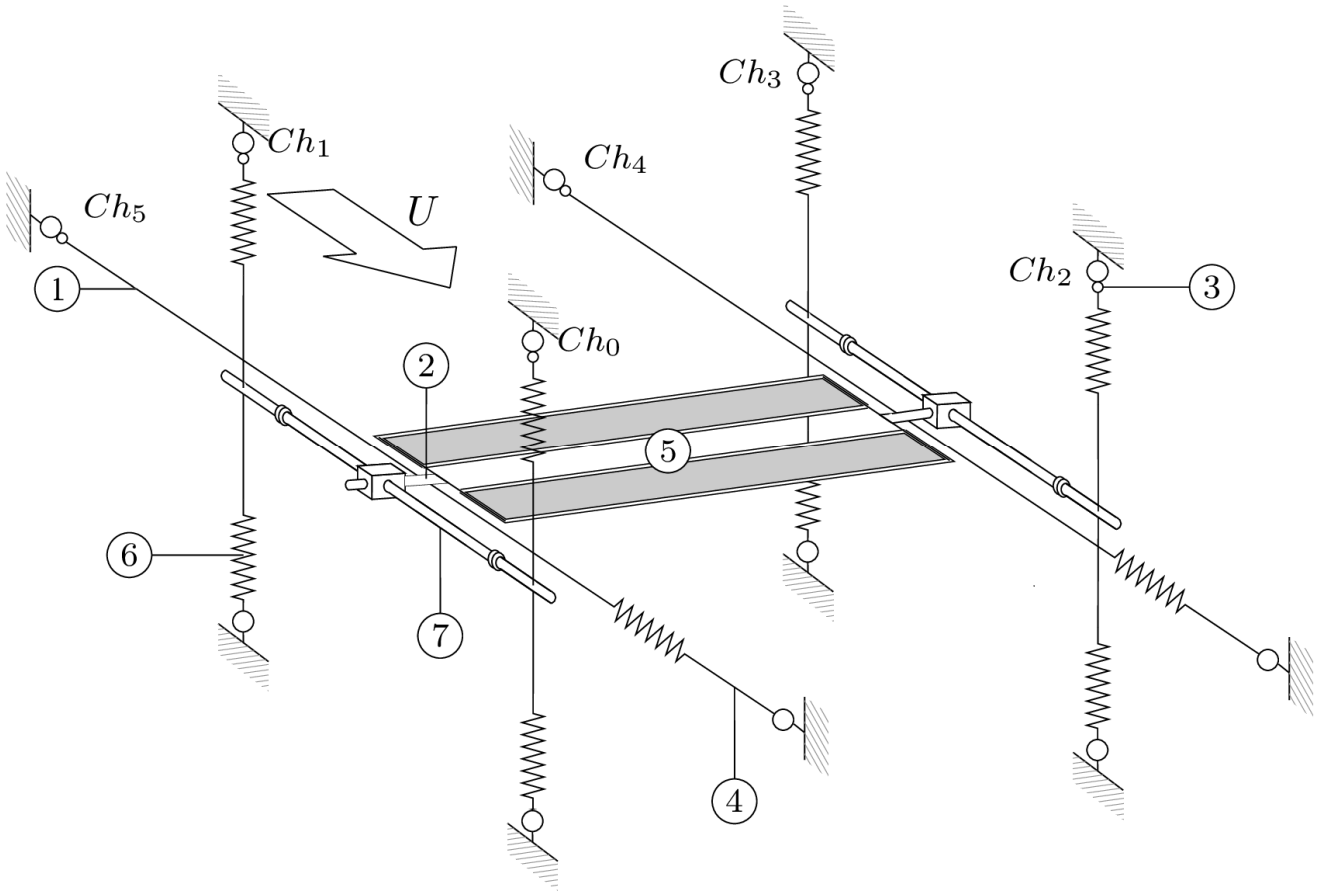

Figure 4: Experimental rig: 1 Wind ward drag wire; 2 Horizontal extension rod; 3 Load cells LC.1 to LC.6; 4 Leeward drag wire with horizontal spring; 5 Section model; 6 Vertical spring; 7 Horizontal bar to connect section model with vertical springs.

The dynamic response of the model was recorded through 6 load cells at a sampling rate $f_s = 500\ Hz$ for 70 seconds. Prior to the tests, the load cells were calibrated, using static weights. A linear least squares approximation was used to determine the voltage-to-force ratio. A total of 8 parallel connected springs was used to suspend the section model. The spring constant of each spring was determined by single degree of freedom tests. The vertical modal stiffness of the section model was the sum of all vertical springs. It was determined to $k_h = 2016.7\ N/m$. The corresponding torsional modal stiffness is $k_\alpha = k_h * e_k^2$. The modal still air frequencies and damping ratios was determined by free decaying vibration tests in still air. An implementation of Prony's method (de Prony, 1795) in the Abravibe Toolbox for Noise & Vibration Analysis (Brandt, 2011a) was used to determine the frequency and damping from the recorded time signals. The Toolbox was slightly modified to allow determination of poles with negative damping at the higher wind velocities. The modal mass and modal mass moment of inertia was determined from the still air modal stiffness and frequencies.

4 RESULTS

The Test Series are presented in Table 1. All wind velocities are reduced non-dimensional velocities defined by $U_r = U/(f_h B)$ where f_h is the *still air* vertical frequency. The highest stable wind velocity observed is denoted U_1 while the lowest instable velocity observed is denoted U_2. Hence, the reduced critical wind velocity U_{cr} is in between U_1 and U_2.

Table 1. Test arrangement for the section model tests

Series	1a	2a	2b	2c
γ_ω	1.20	1.22	0.92	0.99
e_k[m]	0.155	0.200	0.125	0.200
Z [m]	0	0.091	0.091	0.091
f_h [Hz]	1.52	1.52	1.52	1.36
B [m]	0.576	0.667	0.667	0.667
$D:B$	1:24	1:27.8	1:27.8	1:27.8
m_e [kg/m]	13.10	13.08	13.07	16.18
I_e [kg m^2/m]	0.2184	0.3514	0.2457	0.6638
ζ_h [%]	0.51	0.22	0.18	1.12
ζ_α [%]	1.21	0.74	0.36	1.46
ρ [kg/m^3]	1.17	1.17	1.17	1.17
$C_m{}'$	$\pi/2$	0.935	0.935	0.935
U_{CF}	7.94	(7.42)	-	-
$U_{TD,R}$	11.07	17.97	11.23	17.97
U_1	8.09	8.84	10.69	12.03
U_2	8.10	8.92	-	-

4.1 Time histories

Series 1a and Series 2a failed due to classical flutter. The twin boxes in Section 2b rotated at the higher wind velocities. The static torsional displacements were used to calculate the moment coefficients. In Series 2c, the twin boxes were neither prone to flutter nor large static rotations. The vertical and torsional displacement time histories at the critical or at the highest reached wind velocities are presented in Figure 5.

4.2 Aerostatic moment coefficients

The torsional displacement of the section model in Series 2b increased from 0.34° at $U_r = 8.85$ to 1.76° at $U_r = 10.69$. The increasing angle of attack is illustrated in Figure 6 where α is the mean value of the rotation from t=2s to the end of the signal. The marks on the graph passed the runs test of stationarity and the reverse arrangement test based on 33 segments of 1s each at a 0.05 level of significance. The runs and reverse arrangement test is described in e.g. Brandt (2011b). The slope of the fitted line is $C_m{}' = 0.935$.

4.3 Spectral Analysis

In Series 1a and 2a aerodynamic coupling between vertical and torsional modes are clearly observed. In still air, two distinct peaks for vertical and torsional motion appear. Between the still air and the critical wind velocities, the peaks come closer together. The spectra become noisy due to signature turbulence. At the critical wind velocity, the former distinct peaks are merged together in a large peak at a common frequency in-between their still air natural frequencies. In Series 2c the initially decoupled still air modes were further separated by the motion-induced wind load. This might be because of the negative aerodynamic torsional stiffness associated with A_3^*. Series 2b has no distinct torsional frequency above $U_r = 8.8$. Selected transient spectra are presented in Figure 7.

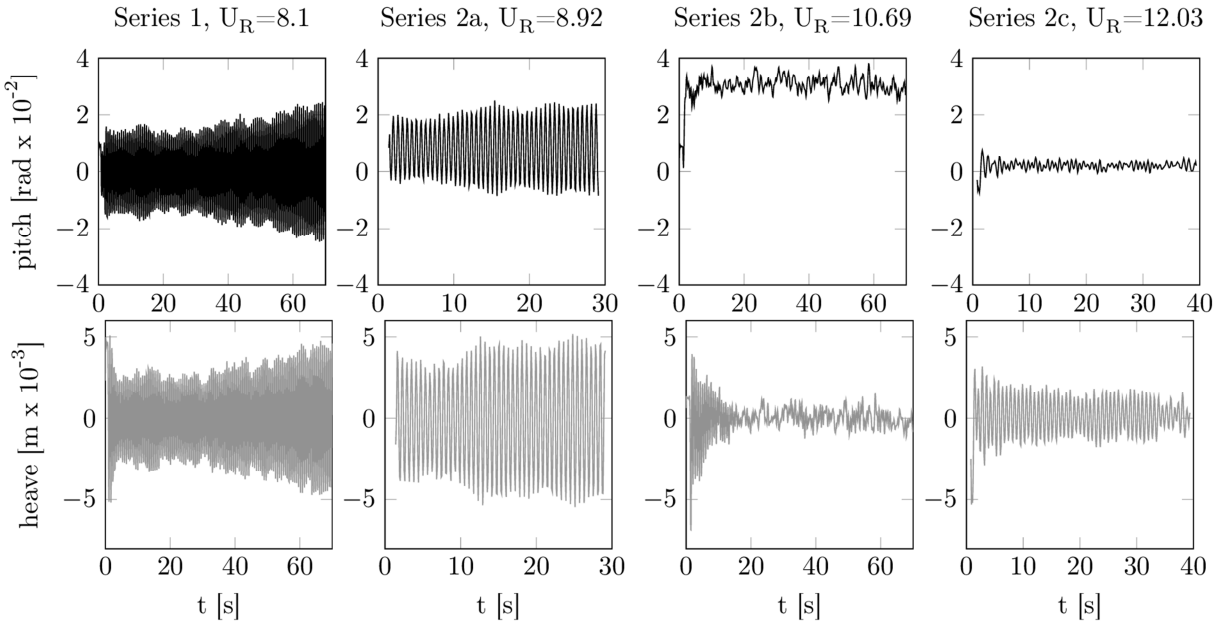

Figure 5: Vertical (heave) and torsional (pitch) time histories

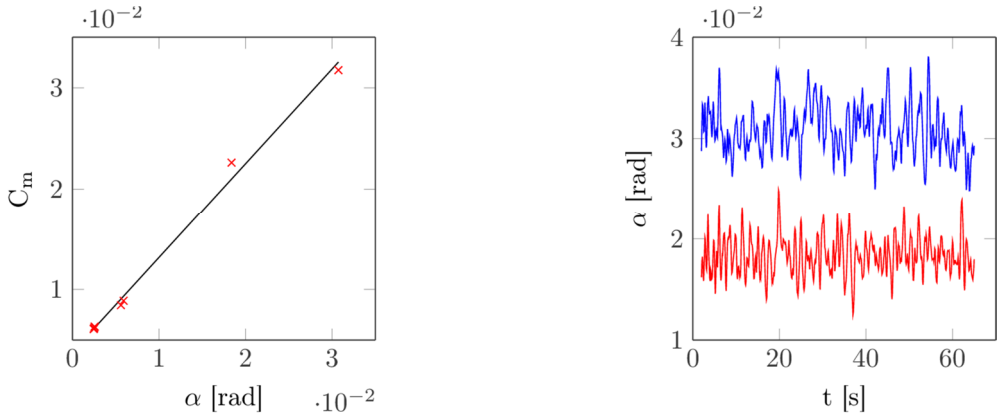

Figure 6: (Left) Moment coefficients for Series 2b at different angles of attack based on the elastic suspended section model at higher wind velocities ($6.88 \leq U_r \leq 10.69$). (Right) Examples of recorded torsional time signals at $U_r = 9.8$ (lower curve) and $U_r = 10.69$ (upper curve) respectively for Series 2b.

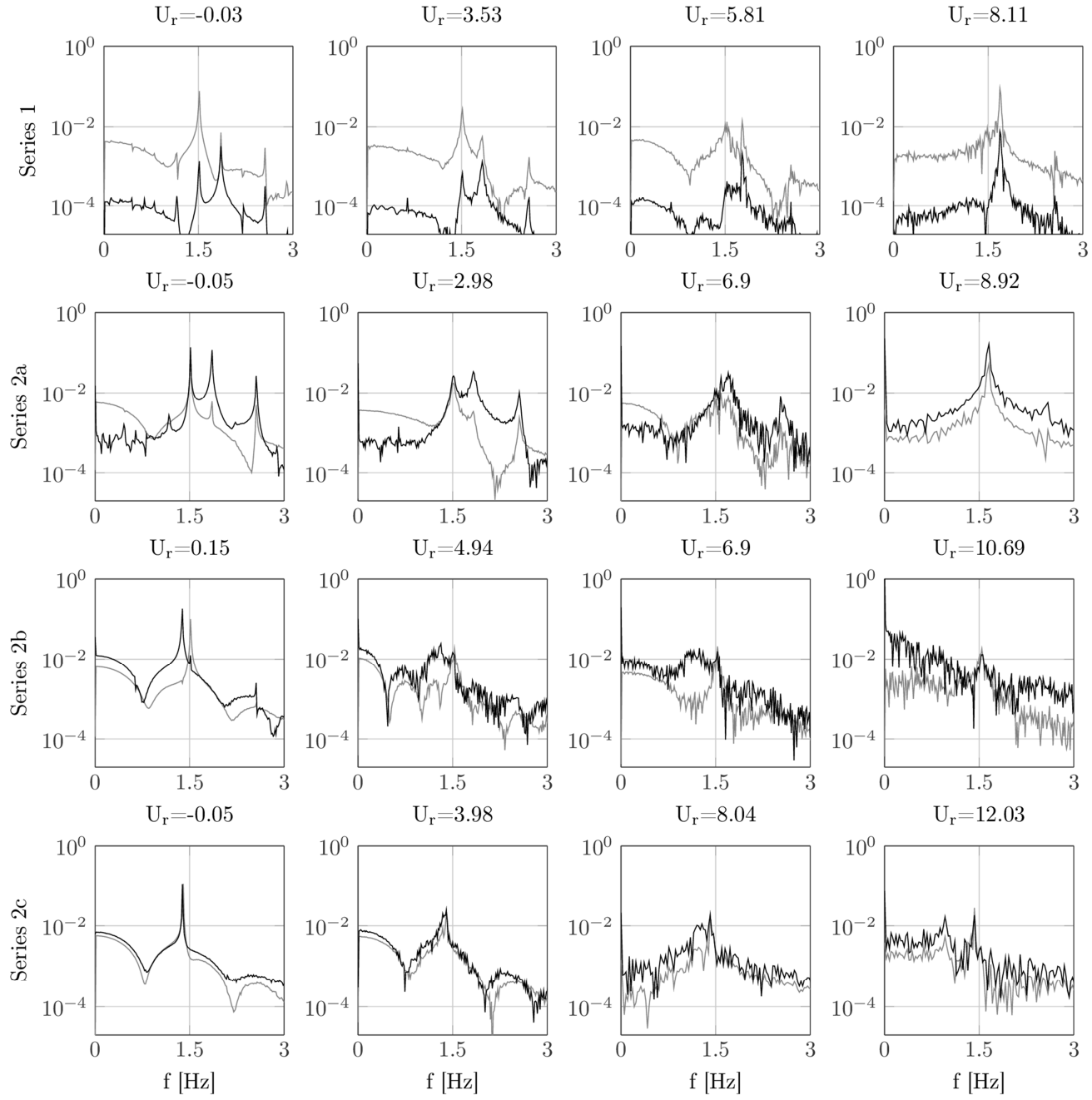

Figure 7: Selected transient spectra. The solid black line is the transient spectrum of the torsional signal and the solid grey line is the transient spectrum of the vertical signal. The units of the ordinate are $rad\ s$ and $m\ s$ for the torsional and vertical signal respectively. The axes are scaled equally in all plots.

4.4 Aerodynamic Derivatives

Aerodynamic Derivatives were identified by the Unifying Least Squares method, described by e.g. Ding et al. (2010) and Gu et al. (2000). In order to reduce the impact of noise on the signals, a 5 Hz low-pass filter was applied. An initial displacement as described in Section 3 was applied to all tests. The signals were cut off when the transient motion of the torsional or vertical signal had died out. The torsional signal was amplified by the weighting constant $w_a = B^2/4$. The AD's are presented in Figure 8 as functions of the reduced wind velocity $U_r = U/(Bf_h)$ for the vertical AD's $H_1^*, A_1^*, H_4^*, A_4^*$ and $U_r = U/(Bf_\alpha)$ for the torsional AD's $H_2^*, A_2^*, H_3^*, A_3^*$ where f_h and f_α are the vertical and torsional frequencies at the wind velocity U.

Increased scatter were observed at higher wind velocities close to the critical flutter wind velocity. This may be caused by non-linear effects due to larger amplitudes and the few cycles of oscillation available at these wind velocities. Increased noise levels were seen in Figure 7 at the higher wind velocities. This may be caused by signature turbulence, which also increase the uncertainties of the AD's.

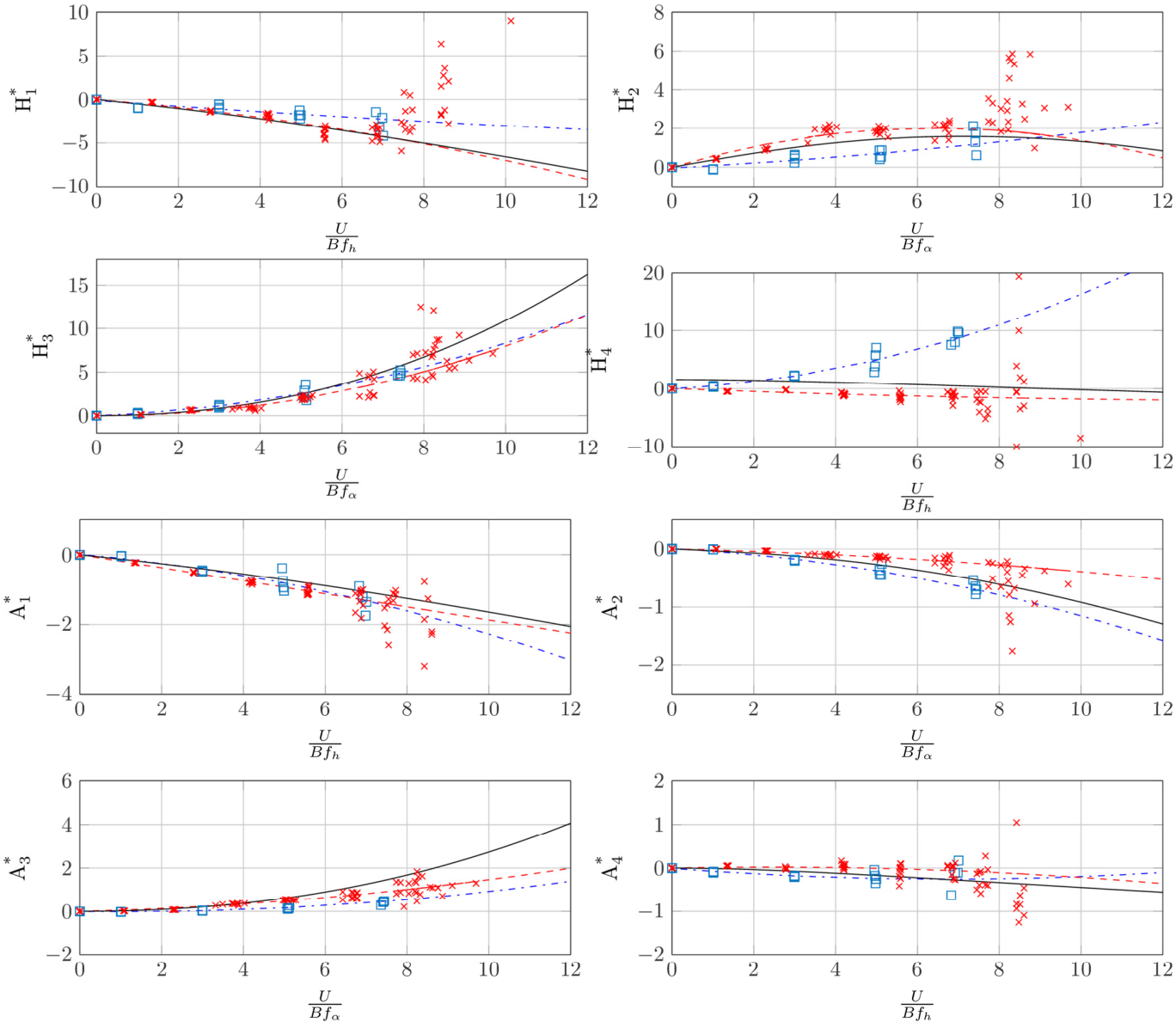

Figure 8: AD's for the reference flat plate and the twin boxes compared with the theoretical flat plate AD's.

× Flat plate AD's (Series 1b), □ Twin boxes AD's (Series 2a), - - - Fitted polynomial to Flat plate AD's, -·- Fitted polynomial to Twin boxes AD's, —— Theoretical flat plate AD's

A least squares polynomial fit, of order n=2, for the AD's as a function of U_r are presented in Table 2. Several synthetic points were inserted in (0; 0) in order to force the curves through that point. Deviations from zero for the coefficients n=0 is considered a systematic error because the motion-induced wind load must be equal to zero in still air. Only AD's below $U_r = 7.01$ and

$U_r = 7.45$ for the vertical and torsional AD's in Series 2a and $U_r = 7.45$ and $U_r = 7.73$ for the vertical and torsional AD's in Series 1b was used in the curve fitting. Extrapolation was used to predict the AD's at higher wind velocities.

Table 2: Polynomial coefficients for the aerodynamic derivatives as a function of the reduced wind velocity

	Flat plate, Series 1b			Twin boxes, Series 2a		
	n=2	n=1	n=0	n=2	n=1	n=0
$H_1^*(U_r)$	-0.0313	-0.3884	0.0095	0.0055	-0.3456	-0.1103
$H_2^*(U_r)$	-0.0491	0.6304	-0.0077	0.0075	0.1082	-0.0392
$H_3^*(U_r)$	0.0834	-0.0378	0.0037	0.0665	0.1672	-0.0017
$H_4^*(U_r)$	0.0086	-0.2666	0.0018	0.1289	0.3426	-0.0183
$A_1^*(U_r)$	0	-0.1873	0.0009	-0.0128	-0.1005	0.0119
$A_2^*(U_r)$	-0.0023	-0.0159	0.0007	-0.008	-0.0356	0.0065
$A_3^*(U_r)$	0.0098	0.0488	-0.0022	0.0118	-0.0259	-0.0014
$A_4^*(U_r)$	-0.0041	0.0196	0.0008	0.0056	-0.0747	-0.0056

Determining the critical flutter velocity from the fitted curves was done as a measure of quality assurance. Series 1a has a critical wind velocity $U_{CL} = 8.08$ based on the coefficients given in Table 2. The observed critical flutter wind velocity was $U_2 = 8.10$. In Series 2a the same accuracy was not obtained. The calculated flutter wind velocity with the AD's identified was $U_{CL} = 16.22$. This result is a large overestimation compared to the observed critical flutter velocity $U_2 = 8.92$. Probably the estimation of the vertical stiffness AD's A_4^* and H_4^* is biased. Setting them equal to zero reduces the flutter wind velocity to $U_{CL} = 10.06$. The estimation of the AD's in Series 2a is based on 15 tests in wind while Series 1b is based on 40. Therefore the accuracy is also expected to be better in Series 1b.

5 CONCLUSIONS

Aerodynamic Derivatives (AD's) for the twin boxes and the flat plate was determined by a Unifying Least Squares method. The general trend of the flat plate AD's follows the theoretical thin airfoil AD's according to Theodorsen (1934). The beneficial effect of a central gap was evident as the critical wind velocity observed compared to the theoretical thin airfoil critical velocity was higher for Series 2a compared with 1a. The values A_3^* and A_2^* were smaller for Series 2a than for Series 1b. This means that the negative torsional aerodynamic stiffness were smaller for the twin boxes while the positive aerodynamic torsional damping were larger. This may be the explanation of the higher critical flutter wind velocities for twin boxes. However, scatter of the AD's at wind velocities close to flutter must be carefully considered when predicting full scale flutter wind velocities.

If the twin boxes have a torsional-to-vertical frequency ratio below unity flutter is prevented, but if the torsional stiffness is reduced in order to obtain low torsional frequencies, static rotations may be expected at high wind velocities. Instead, the mass moment of inertia should be increased and the aerostatic moment coefficients $C_m(\alpha)$ reduced. Such a design would eliminate classic flutter and torsional divergence.

ACKNOWLEDGMENTS

The financial support from the University of Southern Denmark and the hospitality at Svend Ole Hansen Aps is greatly appreciated. Special thanks are extended to Anders Brandt for his advice and guidance on the experimental dynamics and signal analysis.

REFERENCES

Andersen, M. S., Sahin, E., Laustsen, B., Lenius, M. & Røssel, J. (2014, June). *Implementation of the non-flutter design principle*. XIII Conference of the Italian Association for Wind Engineering.

Bartoli, G., D'Asdia, P., Febo, S., Mannini, C., Pastò, S. & Procino, L. (2008). *Innovative Solutions for long-span suspension bridges.* Paper presented at the BBAA VI International Colloquium on: Bluff Bodies Aerodynamics & Applications.

Bleich, F., McCullough, C. B., Rosecrans, R. & Vincent, G. S. (1950). *The mathematical theory of vibration in suspension bridges*: Department of commerce bureau of public roads.

Brandt, A. (2011a). ABRAVIBE -- A MATLAB toolbox for noise and vibration analysis and teaching. http://www.abravibe.com: Department of Technology and Innovation, University of Southern Denmark.

Brandt, A. (2011b). *Noise and vibration analysis - Signal Analysis and Experimental Procedures*: Wiley.

Chowdhury, A. G., & Sarkar, P. P. (2003). A new technique for identification of eighteen flutter derivatives using a three-degree-of-freedom section model. *Engineering Structures, 25*(14), 1763 - 1772.

de Prony, G. R. (1795). Essai éxperimental et analytique: sur les lois de la dilatabilité de fluides élastique et sur celles de la force expansive de la vapeur de l'alkool, à différentes températures. *Journal de l'école Polytechnique*.

Ding, Q., Zhou, Z., Zhu, L. & Xiang, H. (2010). Identification of flutter derivatives of bridge decks with free vibration technique. *Journal of Wind Engineering and Industrial Aerodynamics*.

Dyrbye, C. & Hansen, S. O. (1997). *Wind loads on Structures*: Wiley.

Gu, M., Zhang, R. & Xiang, H. (2000). Identification of flutter derivatives of bridge decks. *Journal of Wind Engineering and Industrial Aerodynamics*.

Johansson, J., Andersen, M. S. & Øvre, M. S. (2013). *Non-flutter design principle for long span bridges.* Proceedings of the Eighth Asia-Pacific Conference on Wind Engineering.

Larsen, A. & Larose, G. (2015). Dynamic wind effects on suspension and cable-stayed bridges. *Journal of Sound and Vibration*.

Qin, X. R., Kwok, K. C. S., Fok, C. H. & Hitchcock, P. A. (2006). Effects of frequency ratio on the aerodynamic and dynamic properties of bridge decks. *Proceedings of the ASME Pressure Vessels and Piping Conference*, 963 - 979.

Qin, X. R., Kwok, K. C. S., Fok, C. H., Hitchcock, P. A. & Xu, Y. L. (2007). Wind-induced self-excited vibrations of a twin-deck bridge and the effects of gap-width. *Wind and Structures, 10*(5), 463 - 479.

Richardson, J. R. (1981). The development of the concept of the twin suspension bridge. *NMI R125*.

Scanlan, R. H., & Tomko, J. J. (1971). Airfoil and Bridge Deck Flutter Derivatives. *Journal of the engineering mechanics division*, 1717-1737.

Theodorsen, T. (1934). General theory of aerodynamic instability and the mechanism of flutter. *NACA Report, 496*, 291-311.

Walshe, D. E., & Wyatt, T. A. (1992). Bridge aerodynamics 50 years after Tacoma Narrows - Part 2: A new discipline world-wide. *Journal of Wind Engineering and Industrial Aerodynamics*.